RSC Advances

ROYAL SOCIETY OF CHEMISTRY

www.rsc.org/advances

RSC Advances

RSCPublishing

ARTICLE

Highly flexible transparent conductive graphene /single-walled carbon nanotube nanocomposite films produced by Langmuir–Blodgett assembly

Cite this: DOI: 10.1039/xoxxoooooox

Received oothxxxxxxxxxxxx,
Accepted oothxxxxxxxxxxxx

DOI: 10.1039/xoxxoooooox

www.rsc.org/

Tan Yang,[a] Junhe Yang,*[a] Lifang Shi,[a] Edith Mäder,[b] and Qingbin Zheng,*[a,b]

Transparent conductive films (TCFs) composed of ultra-large graphene oxide (UL-GO) and functionalized single-walled carbon nanotubes (SWCNTs) are assembled on a flexible poly(ethylene terephthalate) (PET) substrate by using the Langmuir–Blodgett (L–B) technique. After reduced by hydriodic (HI) acid, the TCFs provide excellent optical and electrical properties with a remarkable sheet resistance 8.1 $k\Omega \cdot sq^{-1}$ at a transmittance of 90.3%. It is also found that the deposition of an additional layer of hydrophilic coating on PET substrate could greatly improve the hydrophilicity of PET, which is mainly due to the introduced hydrophilic functional groups and high surface roughness of the coating layer. This highly efficient and self-assembly approach could be used to fabricate TCF devices without post-transfer processes in large-scale.

1. Introduction

Transparent conductive films (TCFs) are essential for many areas of modern electronics, such as displays, touch-panels, light emitting diodes, and solar cells.[1-3] The conventional materials to produce TCFs are indium tin oxide (ITO) and fluorine tin oxide (FTO), which possess high electrical conductivity and optical transparency.[4, 5] However, some problems cannot be ignored when using these films for further applications, such as complex production crafts, high processing cost, inflexibility, and insufficiency of rare metals.[6] Furthermore, the next generation TCF devices require high flexibility, while ITO and FTO are brittle. Owing to the excellent conductivity and mobility, graphene is considered as alternative material to replace ITO and FTO.[7] In comparison with the traditional TCFs, graphene-based TCFs possess high mechanical strength, good chemical stability, low processing cost, easy access to raw materials, and excellent flexibility.[3, 8-10] The first challenge to develop large-area graphene-based TCFs is to produce sufficient amounts of high quality graphene sheets.[11, 12] Among various techniques of synthesizing graphene, including mechanical cleavage,[13] solution exfoliation,[14] epitaxial growth,[15] chemical vapor deposition (CVD),[16] total organic synthesis[17] and reduced graphene oxide (GO),[9, 18] chemical oxidation and reduction method is suitable to achieve industrial production. Since GO dispersions can achieve stable and homogeneous colloidal suspensions in aqueous or polar organic solvents,[3, 10, 19] several well-established techniques, including spin or spray coating,[20, 21] transfer printing,[4, 22] dip coating,[23] electrophoretic deposition,[24] and Langmuir–Blodgett (L–B) assembly,[9, 14, 22, 25] have been developed to deposit GO onto substrates. These typical coating methods are simple and routine to prepare a uniform layer of film by controlling the depositing factors.[11, 26, 27] Among these approaches, L–B assembly is known to be the only technique that can realize the molecule level controlled layer-by-layer deposition,[11,28] which can lead to much lower surface resistance because every layer is parallel with the substrate surface. In our previous work,[3, 9-11] ultra-large GO (UL-GO) or UL-GO/carbon nanotubes (CNTs) TCFs have been assembled on hard substrates such as quartz, delivering outstanding optical and electrical properties. This is because UL-GO can facilitate the restoration of the inherent electrical conductivity with reducing intersheet tunneling barriers, while single-walled CNTs (SWCNTs) can form 3D conductive networks through the film thickness between the GO layers. The synergy effects of combining UL-GO and SWCNTs result in much better optical and electrical properties than only one component. However, assembly of GO based films onto flexible substrates is highly needed for the next-generation flexible electronics.[29]

The polyethylene terephthalate (PET), one of the most widely-used materials in various industries, is a suitable flexible substrate owing to its high optical transparency and flexibility. The key to deposit GO based nanocomposite films onto flexible substrates via L-B technique is producing highly hydrophilic surfaces. However, the hydrophobicity of PET limits its adhesion ability to the GO sheets during L–B assembly. Many approaches, such as plasma treatment,[30, 31] corona discharge,[32] UV/O_3 and irradiation,[33, 34] have been performed to make hydrophilic modification of polymer substrates. However, these methods are either not scalable or hard to achieve the desired hydrophilicity without sacrificing transparency and integrity. One possible way is to deposit one layer of additional hydrophilic thin film with high surface roughness containing hydrophilic group, such as hydroxyl, onto the PET substrate by L–B assembly.[35]

In this study, a simple and scalable treatment method is developed to produce highly hydrophilic PET substrates based on L-B technique. GO and COOH-functionalized SWCNT monolayers are then directly deposited onto the flexible, transparent and hydrophilic PET substrate without later transferring process. The layered architecture of the nanocomposite films and PET surfaces could be accurately controlled by simply varying the L-B

assembly parameters, such as the surface pressure and the pulling speed of the substrate. The final nanocomposite TCFs after hydriodic acid (HI) reduction displayed outstanding opto-electrical properties. The nanocomposite film possesses a sheet resistance of ~8.3 kΩ·sq^{-1} at 90.3% transmittance even without additional doping treatment, demonstrating a simple method to produce transparent, conductive and flexible TCFs.

2. Experimental

2.1 Preparation of UL-GO and functionalized SWCNTs

The preparation and deposition of GO sheets and SWCNTs sheets on a flexible substrate is schematically illustrated in Fig. 1. The materials and the process employed to produce UL-GO and COOH-functionalized SWCNTs were essentially similar with our previous studies.[3, 9] GO was synthesized based on a modified chemical method. NG with a larger lateral size (up to ~800μm) was oxidized to obtain oxidized graphite, followed with thermal shock to obtain expanded graphite (EG). After performing chemical oxidation, the as-prepared GO dispersion with wide size distribution (1~100μm) was sorted into four different groups of sizes via three-step centrifugation,[9, 10] acquiring UL-GO sheets with a mean area of ~50μm. High purity SWCNTs (synthesized by chemical vapor deposition (CVD) and supplied by Chengdu Organic Chem.) with outer diameter ~2-5 nm and length ~5-30 μm (according to the our TEM characterization) were refluxed using a mixture of sulfuric acid and nitric acid (typically 3:1 volume ratio) for 24 h to obtain amphiphilic COOH-functionalized SWCNTs.[3]

2.2 Preparation of hydrophilic PET

0.327 g of cetyltrimethylammonium bromide (CTAB, AR 99%, CIVI-CHEM) and 100 ml of ethanol (absolute, Sigma-Aldrich) were mixed in a three-neck flask equipped with a condenser and stirred for 1 h at room temperature. Then the flask was flushed with N_2 and 7 ml of tetraethylorthosilicate (TEOS, 96% TCI) was added. Subsequently, 3 ml of HCl solution was added into the flask in the nitrogen atmosphere. The mixture was heated to 80 °C and stirred for 2 h. Finally, the solution was evaporated in the fume cupboard to increase the viscosity. Before depositing hydrophilic coating, the PET films were cleaned ultrasonically in acetone, ethanol and DI water respectively and then dried in a vacuum oven for further dip-coating. The PET substrate with thickness ~1.25 mm was clamped to the dipper of the L-B assembly (KSV NIMA, Medium L-B System) in a perpendicular direction and then vertically dipped into the mixed solution at a speed of 13.5 mm/min. After soaking for 5 min, the substrate was pulled out at the same speed. The transfer of the film occurred when the meniscus was spread on the substrate while it was being pulled out. Finally, the PET substrate with hydrophilic coating was dried again in a vacuum oven.

2.3 L–B assembly of UL-GO/SWCNTs nanocomposite films

The UL-GO or SWCNT monolayers were transferred onto the substrate at various stages of compression. The UL-GO and COOH-functionalized SWCNTs (both ~0.1mg/ml) were first transferred to a 1:5 water/methanol mixture respectively. Then the solution was dropped onto the surface of water at a speed of 100 μL·min^{-1} up to a total of 5–10 mL. After stabilized for about 20 min before compression, the hydrophilic PET substrate was vertically dipped into the trough and pulled out at a speed of 0.1 mm/min. After the deposition of each monolayer, the substrate was dried for 30 minutes in an oven at 80 °C to stabilize the adhesion of monolayers with the substrate or previous monolayer films.

2.4 Reduced UL-GO/SWCNT for TCFs

The UL-GO/SWCNT nanocomposite thin films had to be reduced to restore the original sp^2 carbon structure and thus to increase the electrical conductivity. Due to the low glass transition temperatures of flexible substrates including PET, the selection of a proper reducing agent that can be applied at a low temperature is critically important. It is observed that the bubbles appeared when GO films are immersed into $NaBH_4$ and N_2H_4 solution[36] and the GO films were broken down to small debris. However, it can hardly observe any bubbles around the GO film when immersed in a HI acid solution.[10] The film in the HI acid solution maintains its integrity very well even after a long time reaction. Due to the advantages of HI reduction, the substrates with the nanocomposite films soaked in HI inside a beaker for half an hour at 50℃ followed by cleaning in ethyl alcohol to remove excess HI and drying at 60℃ in an oven.

2.5 Characterizations

Water contact angle of the substrate was measured by a KRUSS DSA30 drop shape analysis system (Krüss GmbH, Hamburg Germany). Scanning electron microscope (SEM, FEI CO. Ltd., Quanta FEG) was used to characterize the structure and morphology of UL-GO, SWCNTs and the nanocomposite films. The tapping-mode atomic force microscope (AFM, Scanning Probe Microscope-NanoScope, Digital Instruments) was employed to evaluate the surface morphology of hydrophilic PET and nanocomposite films. The morphology of GO and SWCNT was characterized by high resolution transmission electron microscopy (TEM, FEI TGF 30). For monolayer GO, SWCNT, and one bilayer nanocomposite film, the GO and SWCNT were transferred onto the Cu grid by the same L-B assembly parameters, which are the keys to control the film morphologies. To ensure that the morphology shown in TEM is representative of the morphology of the carbon nanomaterials over the hydrophilic film, the TEM images are compared with the AFM images obtained directly on the PET substrate, showing the similar surface morphologies. Attenuated Total Reflection Fourier transform infrared spectroscopy (ATR-FTIR, Bio-rad FTS 6000) was used to evaluate the functional groups of hydrophilic coating on surface of PET in the near-infrared region (500–4000 cm^{-1}). X-ray diffraction (XRD, Bruker D8-Advance) patterns of NG, oxidized graphite and EG were obtained with Cu Kα (λ=1.5406Å) radiation (40 kV, 30 mA). Raman spectroscopy (Renishaw MicroRaman/Photoluminescence System) was used to analyse the effects of post-treatments on the surface chemistry of nanocomposite films. The UV-Vis spectra of SWCNTs aqueous solution and the transparency of the TCFs were measured by Perkin Elmer Lambda 750 UV-Vis spectrometer. The sheet resistance of the films was measured by the four-point probe method (Scientific Equipment & Services). In order to reduce the contact resistance between the probes and the film surface, the four contact points were coated with silver paste. The elemental compositions and the assignments of the carbon peaks were characterized by the X-ray

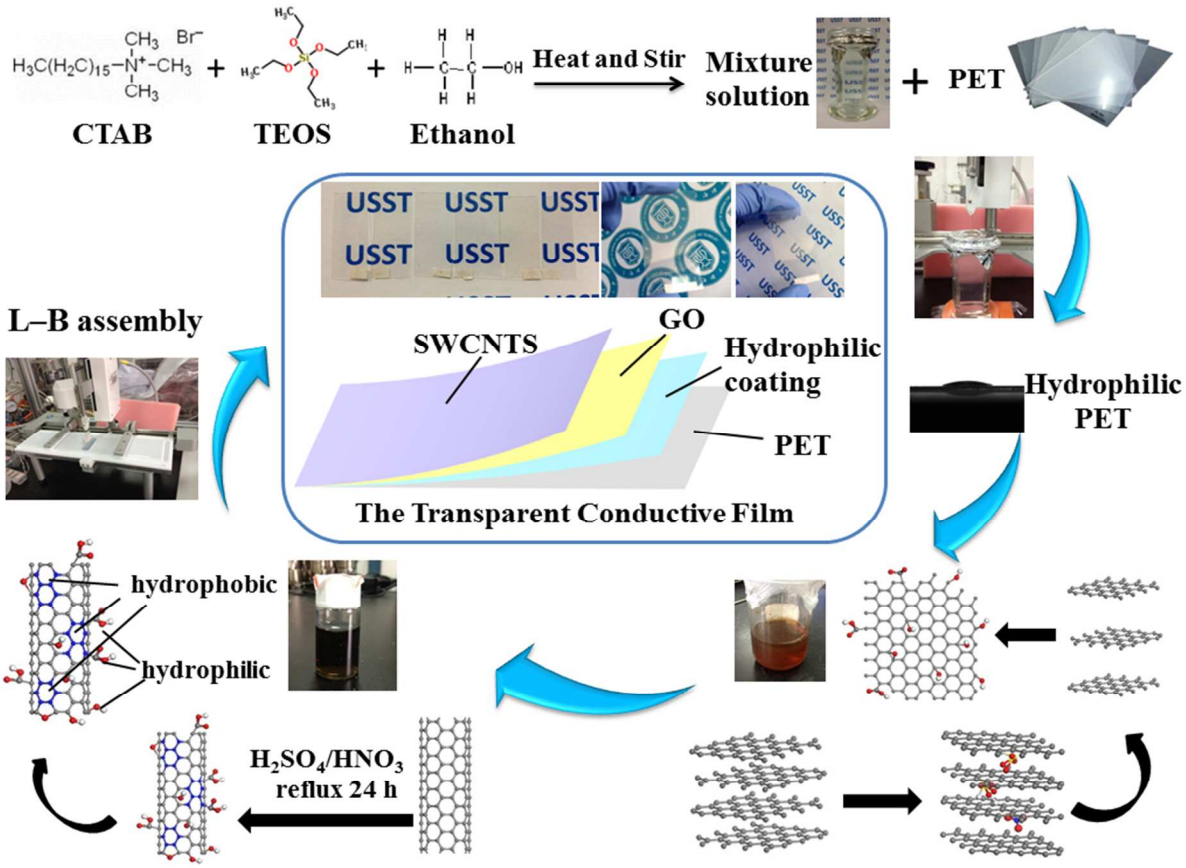

Fig. 1 Flow chart for the synthesis of reduced UL-GO/SWCNT flexible TCFs.

photoelectron 85 spectroscopy (XPS, PHI5600 Physical Electronics), which was equipped with a monochromatic Al Kα X-ray source operated in a residual vacuum of 5×10^{-9} Torr.

3. Results and discussion

3.1 Fabrication of highly hydrophilic PET

As shown in Fig. 1, the TCFs were obtained mainly through two steps, i.e., hydrophilic treatment of the PET substrate by depositing a layer of hydrophilic coating onto the surface via L-B assembly, and synthesis of nanocomposite films by repeatedly depositing the UL-GO and SWCNTs onto the hydrophilic substrates. To obtain the nanocomposite films with uniform coverage and low optical scattering loss, it is important to make PET substrate highly hydrophilic while avoiding the degradation of the excellent flexibility and transparency. As seen in Fig. 2a and b, the hydrophobic surface of as received PET (water contact angle φ=76.1°) became highly hydrophilic (φ=23.1°) after hydrophilic coating was introduced. The significant improvement of hydrophilicity attributes to the surface morphology and chemical structure of the hydrophilic porous silica coating. Typically, CTAB was used as surfactant in the solution and the hydrolysis reaction of TEOS leads to the formation of micelles. Therefore, the viscosity of the final solution is greatly increased after reaction. Hence, the final viscous solution is easy to be transferred to the PET surface upon dipping. Besides, the coating layer formed transparent solid gel and strongly attached to the substrate upon drying.

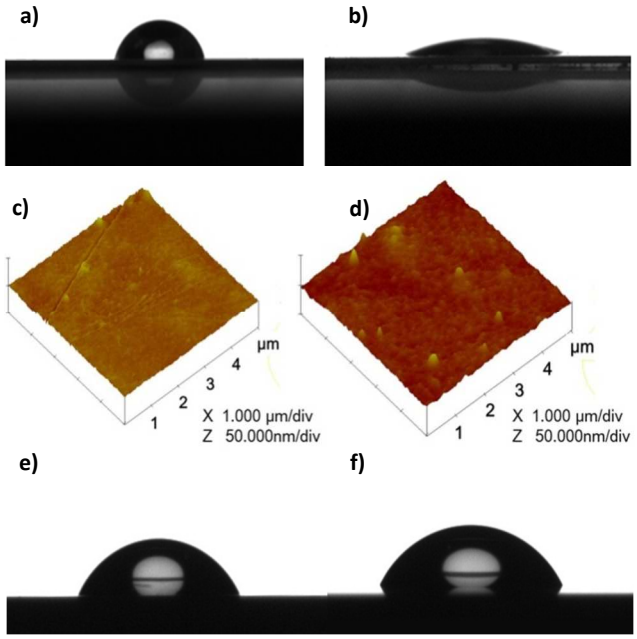

Fig. 2 Water contact angles (a, b) and AFM images (c, d) of PET film before (a, c) and after hydrophilic coating treatment (b, d) (e-f) Water contact angles of PET after depositing one (e) and two (f) bilayers.

It is found that the surface roughness will influence the wettability of PET.[37] As shown in Fig. 2c and d, the root mean squared surface roughness (R_{RMS}) of untreated PET was ~1.46 nm, while a higher R_{RMS} (~2.59 nm) was observed after porous silica coating (around ~300 nm thick, see Fig. S1) was introduced. The higher surface roughness benefits the wettability, and thus leads to good adhesion to the nanocomposite films. In addition, it is worth to mention that the modified dip-coating method by L-B technique can accurately control the dipping speed, which determines thickness uniformity and surface continuity of the hydrophilic coating. The choice of 13.5 mm/min as pulling rate was shown to be the optimum condition to gain a transparent uniform thin film while avoiding cracking on the surface of PET substrate.

To further investigate the chemical structure of the hydrophilic coating layer, XPS and ATR-FTIR spectroscopy were used to characterize the surface functionalities and the elemental compositions. The XPS general spectra and C 1s deconvoluted spectra are presented in Fig. 3a and b respectively. The XPS spectra of the coated PET substrate shows Si 2p, C 1s, and O 1s signals. Both the Si 2p signal at 103.8 eV and the O 1s signal at 533 eV correspond to Si-O in silica gel. As shown in Fig 3b, C–C and C–O functional groups were present in coated PET at binding energies of 285.6, and 286.6 eV respectively. The observation confirms hydrolysis reaction of TEOS and polycondensation and the coverage of the hydrophilic porous silica based thin film.

FTIR peaks corresponding to different functional groups of pristine PET and hydrophilic PET were shown in Fig. 3c. Among them, the band at ~1716 cm^{-1} assigned to the stretching of C=O group in aromatic esters. The band at ~1125 and ~1100 cm^{-1} attributed to the antisymmetric and symmetric stretching of aromatic esters C–O. The broader band from 3200 cm^{-1} to 3700 cm^{-1} for coated PET sample is mainly due to the SiO-H and O-H stretching vibrations. It's obvious that the peaks marginally increased after coating, indicating that many hydrophilic oxygen-containing groups were introduced after coating treatment. Meanwhile, the obvious peak at ~1100 cm^{-1} and a single peak at ~800 cm^{-1} in the spectra of hydrophilic PET attributed to antisymmetric and symmetric stretching of Si-O-Si indicating the formation of silica gel which is consistent with the XPS result.

3.2 L–B assembly of UL-GO/SWCNT nanocomposite films

The key for producing nanocomposite films is synthesis of amphiphilic GO and SWCNT. The UL-GO can be obtained by an approach based on the modified Hummers method.[3, 4, 9] Three main modifications were made to obtain UL-GO, i.e., using the NG with a larger lateral size (up to ~800μm) as starting material, using intercalation and thermal shock to perform exfoliation to avoid the destructive sonication process, and using a three-step centrifugation to sort the GO.[9, 10] The XRD patterns of NG, oxidized graphite and EG are shown in Fig. 4, revealing the different internal structures. The (002) peak at 27° for NG indicates an interlayer spacing of 0.34 nm. The broader peak at 27° after oxidation indicates that some of the graphitic order is lost. Another broad peak of around 12.2° was observed after thermal expansion, indicating that the interplanar spacing is 0.67 nm. GO was obtained by oxidation of EG and UL-GO solution was prepared through three-step centrifugation process.[3, 9] As shown in Fig. S2, the linear relationship between the absorption at the peak for UV-Vis absorbance spectra of the UL-GO solutions and

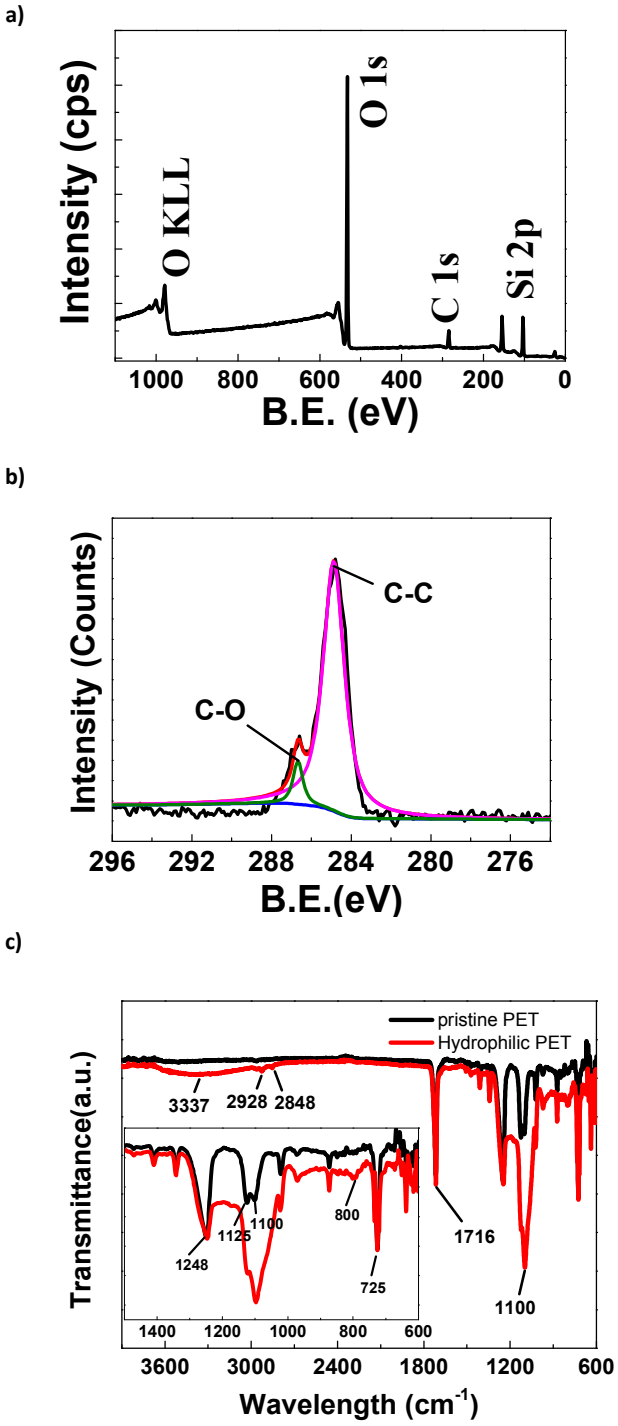

Fig. 3 XPS general spectra of hydrophilic PET for (a) the wide spectra; (b) the C 1s spectra and; and (c) FTIR spectra of pristine PET and hydrophilic PET.

the concentrations of UL-GO indicates good dispersion of UL-GO. The high magnification TEM images of GO (Fig. S3) indicate that the single layer of GO partially collapsed into an amorphous structure, making GO amphiphilic and suitable for L-B assembly.

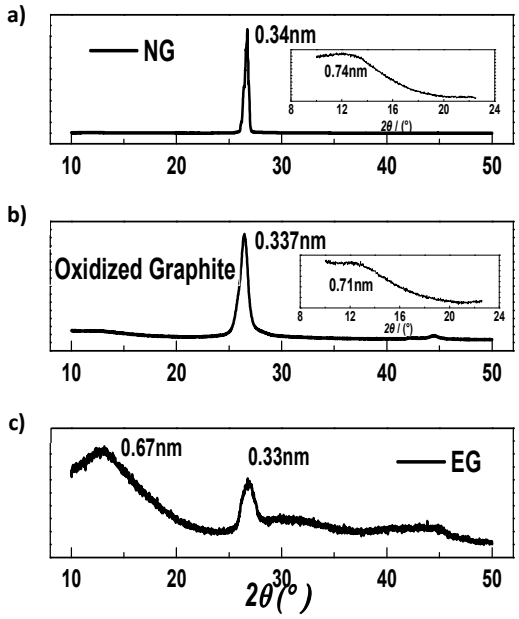

Fig. 4 XRD patterns of (a) nature graphite, (b) oxidized graphite and (c) expanded graphite.

Although surfactant is capable of debundling SWCNT bundles and stabilizing individual tubes, the surfactant molecular is hard to remove, which will greatly reduce the conductivity of the obtained films.[38] To avoid the use of surfactant, the amphiphilic SWCTNs are produced through introducing carboxylic moieties onto the surface non-uniformly, making them amphiphilic and suitable for L–B assembly.[3] Fig. 5a shows the UV-Vis absorbance spectra of the COOH-functionalized SWCNTs aqueous solutions at different concentrations. It was noticed that the absorbance of amphiphilic SWCNTs increases as the concentration increases, which demonstrates the good dispersion of SWCNTs. Fig. 5b shows the linear relationship between the absorption at the peak and the concentration of SWCNTs, indicating that the SWCNTs solution also obey Beer's law. Since the simplest polar protic alcohol, i.e. methanol, was found suitable for spreading the functionalized SWCNTs on the water surface,[3] the functionalized SWCNTs were dispersed in a 1:3 water/methanol solution for L-B assembly. The typical surface pressure–area isotherm curve is shown in Fig. S4. Close packed UL-GO (Fig 6a) and SWCNT monolayers (Fig 6b) were then transferred onto PET substrate by L–B assembly via a layer-by-layer manner.

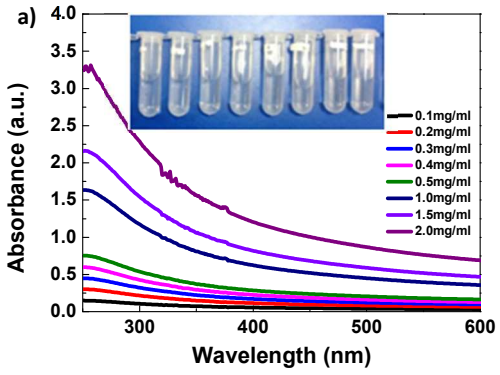

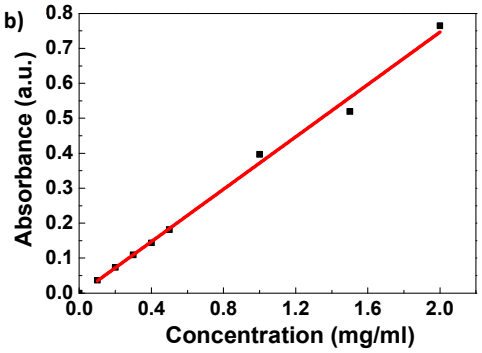

Fig. 5 (a) UV-Vis spectra of –COOH functionalized SWCNT dispersed in water at varied concentrations. (b) Absorption at the peak as a function of the concentration of SWCNT.

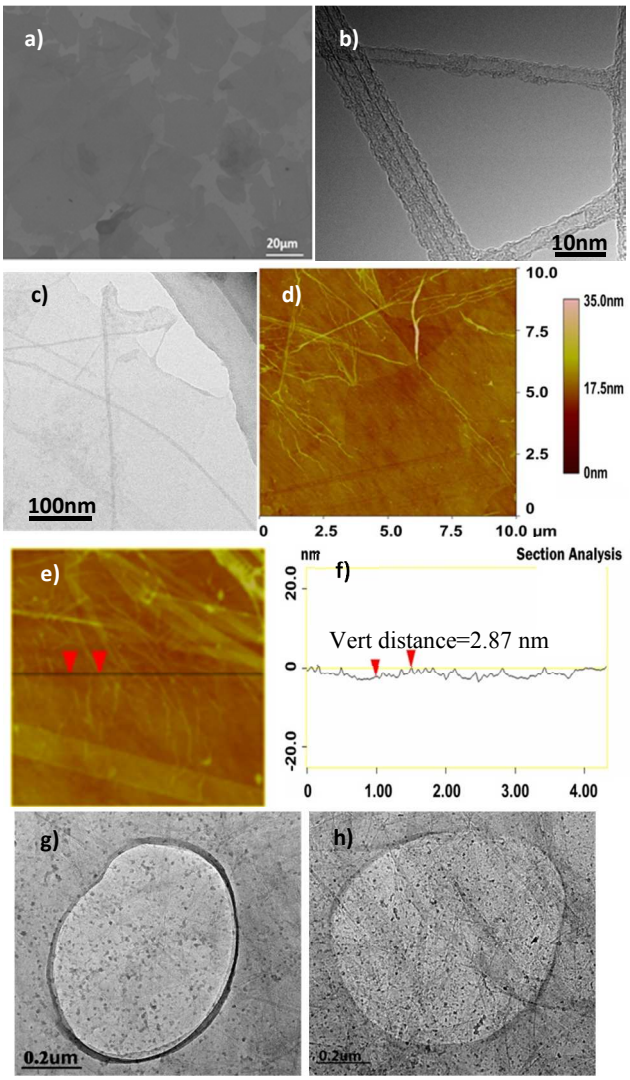

Fig. 6 Morphology of the UL-GO, SWCNTs and their nanocomposite: (a) SEM image of the UL-GO films, (b) TEM image of the SWCNTs films, (c) TEM image of the nanocomposite films, (d, e) AFM images of the nanocomposite films on SiO_2 substrate, and (f) the height profile for the black line in (e), and 2 (g) and 3 (h) bilayers of nanocomposite films.

Figure 6a shows that the size of GO used for L-B assembly is ~50 μm. Figure 6b confirms that monolayer SWCNT forms linked conducting network. Due to the strong bonding through π-π interactions and the amphiphilic nature of both GO and SWCNT surfaces, the GO layer and SWCNT layer were bonded together tightly (Fig 6c and d). The AFM image (Fig. 6d and e) confirmed that there are no aggregates in the SWCNT monolayer produced by L–B assembly. The average height of one bilayer GO/SWCNT nanocomposite film was just over ~3 nm, with occasionally higher peaks due to the wrinkles in the GO sheets. The water contact angle of PET surface was increased to ~60° after depositing one bilayer of UL-GO/SWCNT coating (See Fig. 2e), which is mainly due to the unoxidized surfaces of GO and SWCNT. As the increase of bilayers numbers, the contact angle became slightly higher (~71˚ for two bilayers See Fig. 2f), which may be caused by the increased surface roughness. It is noticed that SWCNTs can not only bridge the GO sheets (Fig 6c-e), but also able to link the GO sheet through thickness, forming 3D nanocomposite films (Fig 6 g-h).

3.3 Reduced GO/SWCNT for TCFs

It is known that the presence of oxygen-containing functional groups hinder charge transport through the atomically thin plane due to the absence of percolating pathways among sp^2 carbon clusters. Hence, the prerequisite for the use of GO/SWCNT nanocomposite film as a TCF is the efficient reduction to restore the sp^2 conjugated network. It is found that GO film in the HI acid solution can maintain its integrity with highly efficient reduction.[36] Due to the advantages of HI reduction, the nanocomposite films were reduced by using HI acid in low temperature to keep the flexibility of the films. The XPS analysis was performed to evaluate the elemental compositions and the functionalities of the nanocomposite films, and thus to better understand their surface chemistries that are directly correlated to the optical and electrical properties. The deconvoluted XPS spectra provide further evidence of the reduction. As shown in Fig. 7, the C1s signal mainly consisted of five different chemically shifted components that can be deconvoluted into: C=C (sp^2) at ~284.8 eV; C-C (sp^3) at ~285.6 eV; C-O at ~286.6 eV; C=O at 287.8 eV; and O-C=O at ~290.3 eV. As shown in Table S1, the components of the C-O, C=O and O-C=O functional groups had 29.49%, 17.69% and 2.29% of the carbon signal in the GO/SWCNT nanocomposite films before reduction, which were subsequently reduced to 13.10%, 12.73% and 1.92% respectively after the HI treatment.

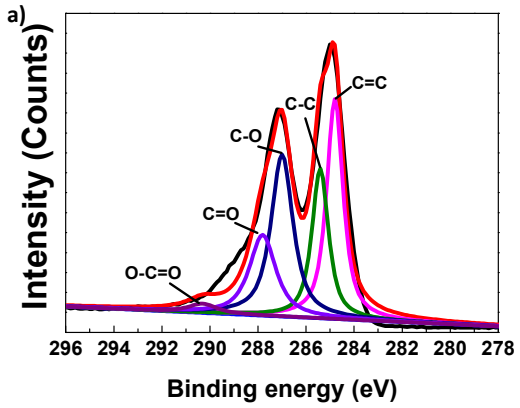

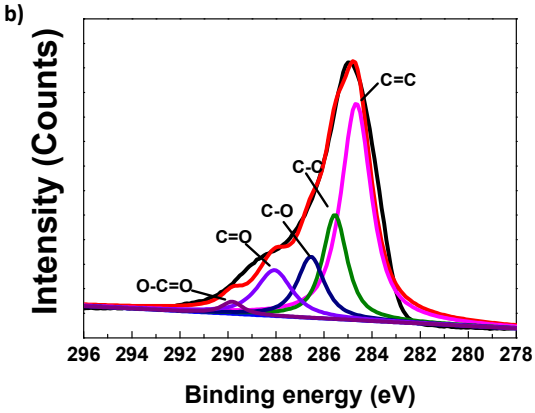

Fig. 7 XPS general spectra and curve fitting of C1s spectra of GO/SWCNT nanocomposite films before(a) and after(b) HI reduction.

The Raman spectra of the GO, SWCNTs, and the GO/SWCNT nanocomposite films directly reveal the degree of disorder and the stacking structure of the graphitic framework. Raman spectra of natural graphite, EG and UL-GO is shown in Fig. S5a. Due to the destructive chemical oxidation, the G-band peak of UL-GO was up-shifted from 1581 to 1601 cm^{-1}. The intensity ratio of I_D/I_G for UL/GO is also greatly increased compared with graphite and EG. Raman spectra of SWCNT before and after functionalization are shown in Fig. S5b. The bands near 1284 cm^{-1} were observed after oxidation, which present the sp^3-hybrized carbon in the hexagonal framework of the SWCNT walls, indicating covalent attachment (such as -COOH) after oxidation.[39] Fig. 8 presents the micro-Raman spectra of the UL-GO/SWCNT nanocomposite thin film before and after HI reduction. The relative intensities of the D and G peaks are almost the same after HI treatment, indicating that defects and other types of functionalization are simultaneously introduced upon reduction.[40]

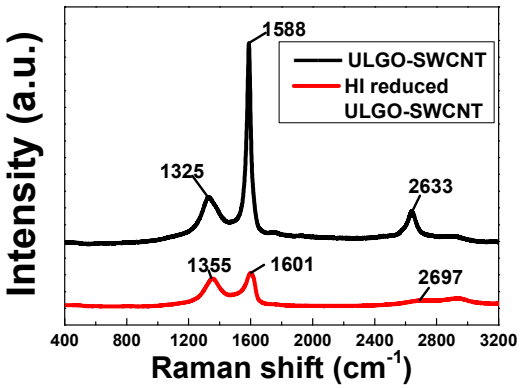

Fig. 8 Raman spectra for GO /SWCNT nanotube nanocomposite films before and after HI reduced.

Fig. 9a presents the UV–Vis spectra of nanocomposite films with different thicknesses, showing the changes in transmittance in the wavelength ranging from 400 to 1000 nm. As expected, the

transparency of the film decreased with increasing film thickness (Fig. 9b). The increase in thickness increased both the back reflection and absorption of light, resulting in the reduction in transparency. Since thicker nanocomposite films with lower transparencies form better 3D conducting network, the sheet resistance increases with optical transmittance (Fig 9c). The ratio of DC to optical conductivity, i.e., σ_{DC}/σ_{Op}, can be used as a figure of merit for comparisons between TCFs with different transparencies and conductivities.[11] The DC to optical conductivity ratio of the reduced nanocomposite film can reach up to 0.443 at 90.3% transmittance, showing outstanding optical and electrical performance among solution based methods (See Table S2) to produce flexible TCFs.

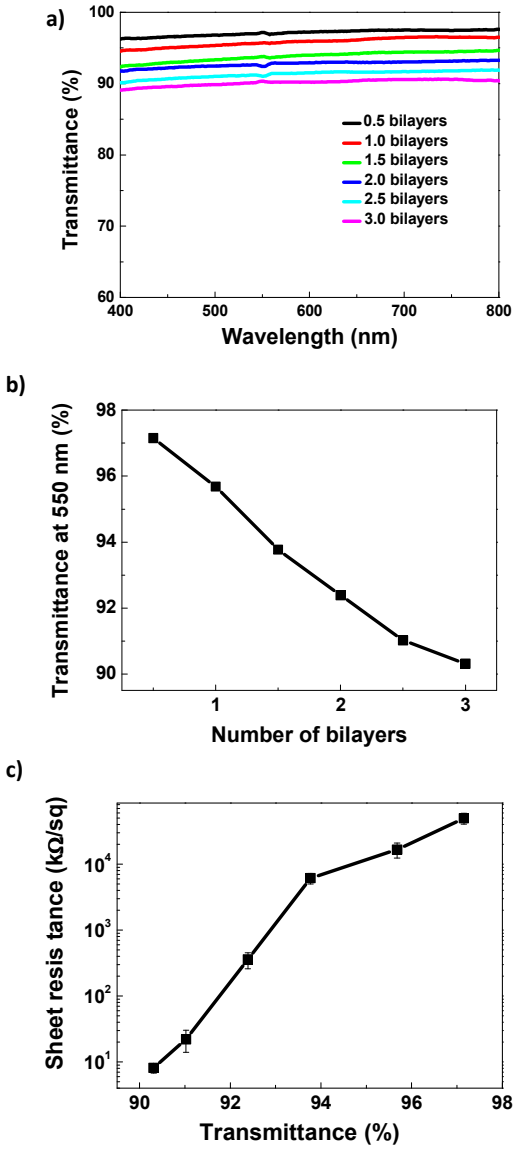

Fig. 9 Optical and electrical properties of the rUL-GO/SWCNT nanocomposite flexible films with different bilayers: (a) transmittance spectra of nanocomposite films, (b) transmittance measured at 550 nm wavelength, and (c) sheet resistance versus transmittance.

4. Conclusions

A synthesis method is developed based on layer-by-layer deposition of molecular-scale carbon layers using the well-established L-B assembly without an intermediate transfer process to produce highly conductive flexible TCFs. The nanocomposite film possesses a sheet resistance of ~8.3 $k\Omega \cdot sq^{-1}$ at 90.3% transmittance even without additional doping treatment. The proposed process offers the following advantages over existing techniques: namely, (i) the PET hydrophilic treatment by dip-coating is simple and effective, which is suitable for industrial mass production; (ii) the L-B technique is easy and convenient for the assembly of nanocomposite films directly on the hydrophilic coating surface; (iii) the demonstrated L-B assembly method to produced GO based hybrid TCFs is simple and suitable for large-scale fabrication.

Acknowledgements

The authors gratefully acknowledge financial support from NSFC (51102170, 51272157), Shanghai Pujiang Talent Project (13PJ1406400), China Postdoctoral Science Foundation (2012M520912), Shanghai Postdoctoral Science Foundation (13R21415500), Shanghai Committee of Science and Technology (12JC1406900), the Alexander von Humboldt Foundation and the Innovation Fund Project For Graduate Student of Shanghai (JWCXSL1401). The authors thank Dr. S.L. Gao, Dr. H.S. Qi, Dr J.W. Liu, Dr. C. Scheffler, and Dr. U. Gohs at IPF for stimulating discussion.

Notes and references

[a]*School of Materials Science and Engineering, University of Shanghai for Science and Technology, Shanghai 200093, China.Tel.: 86-21-55274065 E-mail address:qingbin.zheng@family.ust.hk (Q.B. Zheng) jhyang@usst.edu.cn (J.H. Yang)*

[b]*Leibniz-Institut für Polymerforschung Dresden, Hohe Straße 6, 01069 Dresden, Germany.Tel.: 49-0351-4658486*

† Electronic Supplementary Information (ESI) available: UV–vis spectra of UL-GO dispersed in water at varied concentrations and absorption at the peak as a function of the concentration of UL-GO, TEM images of the oxidized SWCNTs, surface pressure (π) vs area curve of the formation of SWCNTs monolayers in L-B assemly, relative percentages of carbon and assignations of UL-GO/SWCNT and rUL-GO/SWCNT, comparison of opto-electrical properties for TCFs made by solution based methods. See DOI: 10.1039/b000000x/

References

1. Z. C. Wu, Z. H. Chen, X. Du, J. M. Logan, J. Sippel, M. Nikolou, K. Kamaras, J. R. Reynolds, D. B. Tanner, A. F. Hebard and A. G. Rinzler, *Science*, 2004, **305**, 1273-1276.
2. X. Wang, L. J. Zhi, N. Tsao, Z. Tomovic, J. L. Li and K. Mullen, *Angew Chem Int Edit*, 2008, **47**, 2990-2992.
3. Q. Zheng, B. Zhang, X. Lin, X. Shen, N. Yousefi, Z.-D. Huang, Z. Li and J.-K. Kim, *Journal of Materials Chemistry*, 2012, **22**, 25072.
4. Q. B. Zheng, M. M. Gudarzi, S. J. Wang, Y. Geng, Z. G. Li and J. K. Kim, *Carbon*, 2011, **49**, 2905-2916.
5. B. T. Liu, C. H. Hsu and W. H. Wang, *J Taiwan Inst Chem E*, 2012, **43**, 147-152.
6. G. Z. Xiao, Y. Tao, J. P. Lu and Z. Y. Zhang, *Thin Solid Films*, 2010, **518**, 5032-5032.

7. A. K. Geim and K. S. Novoselov, *Nat Mater*, 2007, **6**, 183-191.
8. Y. W. Zhu, S. Murali, W. W. Cai, X. S. Li, J. W. Suk, J. R. Potts and R. S. Ruoff, *Adv Mater*, 2010, **22**, 5226-5226.
9. Q. B. Zheng, W. H. Ip, X. Y. Lin, N. Yousefi, K. K. Yeung, Z. G. Li and J. K. Kim, *Acs Nano*, 2011, **5**, 6039-6051.
10. L. Shi, J. Yang, Z. Huang, J. Li, Z. Tang, Y. Li and Q. Zheng, *Applied Surface Science*, 2013, **276**, 437-446.
11. Q. Zheng, Z. Li, J. Yang and J.-K. Kim, *Progress in Materials Science*, 2014, **64**, 200-247.
12. D. Konatham and A. Striolo, *Nano Lett*, 2008, **8**, 4630-4641.
13. K. S. Novoselov, D. Jiang, F. Schedin, T. J. Booth, V. V. Khotkevich, S. V. Morozov and A. K. Geim, *P Natl Acad Sci USA*, 2005, **102**, 10451-10453.
14. X. L. Li, G. Y. Zhang, X. D. Bai, X. M. Sun, X. R. Wang, E. Wang and H. J. Dai, *Nat Nanotechnol*, 2008, **3**, 538-542.
15. P. W. Sutter, J. I. Flege and E. A. Sutter, *Nat Mater*, 2008, **7**, 406-411.
16. K. S. Kim, Y. Zhao, H. Jang, S. Y. Lee, J. M. Kim, K. S. Kim, J. H. Ahn, P. Kim, J. Y. Choi and B. H. Hong, *Nature*, 2009, **457**, 706-710.
17. X. Y. Yang, X. Dou, A. Rouhanipour, L. J. Zhi, H. J. Rader and K. Mullen, *J Am Chem Soc*, 2008, **130**, 4216-4217.
18. S. Stankovich, D. A. Dikin, R. D. Piner, K. A. Kohlhaas, A. Kleinhammes, Y. Jia, Y. Wu, S. T. Nguyen and R. S. Ruoff, *Carbon*, 2007, **45**, 1558-1565.
19. D. R. Dreyer, S. Park, C. W. Bielawski and R. S. Ruoff, *Chem Soc Rev*, 2010, **39**, 228-240.
20. S. Watcharotone, D. A. Dikin, S. Stankovich, R. Piner, I. Jung, G. H. B. Dommett, G. Evmenenko, S. E. Wu, S. F. Chen, C. P. Liu, S. T. Nguyen and R. S. Ruoff, *Nano Lett*, 2007, **7**, 1888-1892.
21. P. Blake, P. D. Brimicombe, R. R. Nair, T. J. Booth, D. Jiang, F. Schedin, L. A. Ponomarenko, S. V. Morozov, H. F. Gleeson, E. W. Hill, A. K. Geim and K. S. Novoselov, *Nano Lett*, 2008, **8**, 1704-1708.
22. S. J. Wang, Y. Geng, Q. B. Zheng and J. K. Kim, *Carbon*, 2010, **48**, 1815-1823.
23. X. Wang, L. J. Zhi and K. Mullen, *Nano Lett*, 2008, **8**, 323-327.
24. V. Lee, L. Whittaker, C. Jaye, K. M. Baroudi, D. A. Fischer and S. Banerjee, *Chem Mater*, 2009, **21**, 3905-3916.
25. L. J. Cote, F. Kim and J. X. Huang, *J Am Chem Soc*, 2009, **131**, 1043-1049.
26. O. Parlak, A. Tiwari, A. P. F. Turner and A. Tiwari, *Biosens Bioelectron*, 2013, **49**, 53-62.
27. O. Parlak, A. P. F. Turner and A. Tiwari, *Adv Mater*, 2014, **26**, 482-486.
28. J. K. Wassei and R. B. Kaner, *Mater Today*, 2010, **13**, 52-59.
29. S. Bae, H. Kim, Y. Lee, X. F. Xu, J. S. Park, Y. Zheng, J. Balakrishnan, T. Lei, H. R. Kim, Y. I. Song, Y. J. Kim, K. S. Kim, B. Ozyilmaz, J. H. Ahn, B. H. Hong and S. Iijima, *Nat Nanotechnol*, 2010, **5**, 574-578.
30. X. Y. Lin, J. J. Jia, N. Yousefi, X. Shen and J. K. Kim, *J Mater Chem C*, 2013, **1**, 6869-6877.
31. G. Poletti, E. Orsini, A. Raffaele-Addamo, C. Riccardi and E. Selli, *Applied Surface Science*, 2003, **219**, 311-316.
32. W. W. Huang and J. H. Jang, *Fiber Polym*, 2009, **10**, 27-33.
33. P. Khanchaitit and D. Aht-Ong, *Polym Composite*, 2006, **27**, 484-490.
34. J. H. Jang and Y. J. Jeong, *Dyes Pigments*, 2006, **69**, 137-143.
35. B. G. Kum, Y. C. Park, Y. J. Chang, J. Y. Jeon and H. M. Jang, *Thin Solid Films*, 2011, **519**, 3778-3781.
36. S. F. Pei, J. P. Zhao, J. H. Du, W. C. Ren and H. M. Cheng, *Carbon*, 2010, **48**, 4466-4474.
37. J. Skvarla, T. Luxbacher, M. Nagy and M. Sisol, *Acs Appl Mater Inter*, 2010, **2**, 2116-2127.
38. Y. Wang, C. A. Di, Y. Q. Liu, H. Kajiura, S. H. Ye, L. C. Cao, D. C. Wei, H. L. Zhang, Y. M. Li and K. Noda, *Adv Mater*, 2008, **20**, 4442-4449.
39. R. Haggenmueller, F. M. Du, J. E. Fischer and K. I. Winey, *Polymer*, 2006, **47**, 2381-2388.
40. I. K. Moon, J. Lee, R. S. Ruoff and H. Lee, *Nat Commun*, 2010, **1**, 2041-1723.